A Bandwidth Efficient Dual-Function Radar Communication System Based on a MIMO Radar Using OFDM Waveforms

Zhaoyi Xu, *Graduate Student Member, IEEE*, and Athina Petropulu, *Fellow, IEEE*

***Abstract*—A novel dual-function radar communication (DFRC) system is proposed, that achieves high communication rate, and can flexibly trade-off rate for improved sensing performance. The proposed system is a monostatic multiple-input multiple-output (MIMO) radar and transmits wideband, precoded, orthogonal frequency division multiplexing (OFDM) waveforms from its antennas. The system subcarriers are divided into two groups, i.e., shared and private. On a shared subcarrier, all antennas can transmit simultaneously, while on a private one only one antenna can transmit at a time. The shared use of subcarriers by the transmit antennas results in coupling of transmitted symbols and radar target parameters in the target echoes. A novel, low complexity target estimation approach is proposed to overcome the coupling and recover the radar parameters. The proposed method first operates on all (shared and private) subcarriers to obtain coarse angle estimates, and then by fine-tunes those estimates based on the signal received on the private subcarriers. The resolution of the coarse angle estimates is limited by the aperture of the physical receive array, while the fine-tuning is enabled by effectively constructing a virtual array that has larger aperture than the receive array. The precoding matrix is optimally designed to optimize a weighted combination of the beampattern error with respect to a desired beampattern, and the signal-to-noise ratio at the communication receiver.**

***Index Terms*—DFRC system, MIMO radar, OFDM radar waveforms, subcarrier sharing.**

I. Introduction

NEXT-GENERATION wireless networks will support pervasive communication, sensing, connectivity and intelligence in a seamless manner [1]. An emerging trend in 6G wireless applications [2] is to increase spectral efficiency by providing unconstrained spectrum access to radar and communication systems. This trend has given rise to intense interest in enabling spectral *coexistence* of independent radar and communication systems by handling interference [3], [4], [5]. Another form of spectral coexistence is by integrating sensing and communication functions on the same hardware platform. The integration is facilitated by today's technology, where radio frequency (RF) front-end architectures are basically the same in radar and wireless communication systems. In addition to hardware convergence, there is also frequency convergence; by seeking high bandwidth, wireless communication systems have been moving into higher frequency bands that have been traditionally occupied by radar systems. Integrated sensing-communication (ISC) systems offer the potential for significant performance enhancement for both sensing and communications functions [6], [7], [8], [9]. In scenarios with a large number of sensors and communication transceivers, the integration of radar and communication functionalities in one system would reduce device size, power consumption and cost, and would create less interference to network users. Due to these advantages, ISC systems are currently being investigated in many next-generation systems, including intelligent vehicular networks [10], [11] and the Internet of Things (IoT) [12], [13], [14], [15], [16], [17].

Dual-Function Radar Communication (DFRC) systems [17], [18], [19], [20], [21], [22] is a class of ISC systems that use the same waveform as well as the same hardware platform for both sensing and communication purposes simultaneously. Their advantages stem from their ability to achieve high spectrum efficiency as well as hardware reuse. DFRC systems hold great promise for autonomous systems such as future networked autonomous vehicles, or unmanned aerial vehicles (UAV) [23].

Depending on the design priority, DFRC systems can be categorized into three classes [6], namely, radar-centric [24], [25], [26], [27], [28], [29], [30], communication-centric [10], [19], [31], and jointly optimized [32], [33], [34]. Radar-centric systems convey information via the way the radar waveforms are paired with the transmit antennas [24], [25], [26], [27], or in the phase of the sidelobes of the array beampattern [28], or in the antenna activation pattern [29], [30]. Communication information can also be directly embedded in the radar waveforms [8], [26], [30], [35], [36], [37], [38], [39], [40], [41]. Radar-centric systems can have near optimum radar sensing performance but their communication rate is limited. In communication-centric systems [10], [19], [31] the sensing functionality is based on modulated communication waveforms, where 802.11ad standard waveforms have been investigated [10], [11], [31], [42]. The joint optimization design aims to achieve a trade-off between radar and communication performance [32], [33], [34], [43] via

Manuscript received 28 February 2022; revised 13 October 2022 and 7 January 2023; accepted 28 January 2023. Date of publication 6 February 2023; date of current version 28 February 2023. The associate editor coordinating the review of this manuscript and approving it for publication was Prof. Lin Bai. This work was supported by NSF under Grant ECCS-2033433. *(Corresponding author: Athina Petropulu.)*

The authors are with the Department of Electrical and Computer Engineering, Rutgers University, Piscataway, NJ 08854 USA (e-mail: zhaoyi.xu@rutgers.edu; athinap@rutgers.edu).

Digital Object Identifier 10.1109/TSP.2023.3241779

the use of a precoder that is designed to minimize some joint sensing-communication metric, such as the Cramér–Rao bound (CRB) of radar parameters and the communication channel capacity [32], or the CRB and mutual information (MI) for sensing and the communication sum rate [34], or the communication signal-to-interference-plus-noise ratio (SINR) and the beampattern error [33], [43].

High communication rate is highly desirable in the potential applications of DFRC systems. For that reason, the study of the radar sensing properties of multi-carrier waveforms, which are known to achieve high communication rates has attracted a lot of interest. Multi-carrier waveforms with Frequency-Hopping (FH) were proposed in [26], [27], where the bandwidth is divided into multiple subbands, a subset of subbands is randomly selected in each channel use, and each selected band is paired with a transmit antenna. However, this type of subband assignment uses only part of the available bandwidth, which negatively impacts target range resolution and communication rate. Given the popularity of Orthogonal frequency division multiplexing (OFDM) waveforms in high-rate communications, and also their ability to effectively deal with frequency selective fading [44], [45], [46], there has been intense interest in the radar sensing properties of OFDM signals. OFDM waveforms for DFRC systems have been explored in [8], [36], [40], [41], [47], [48], [49]. In those works, non-overlapping subcarriers are assigned to transmit antennas in each channel use. As compared to FH methods, OFDM methods use all available bandwidth for sensing, which allows for higher range resolution. Also, since all subcarriers are used they achieve higher communication rate. However, since each antenna is restricted to transmit on certain subcarriers only, the communication bandwidth is still not fully exploited.

In this paper, we propose a novel OFDM-based DFRC system that uses the available bandwidth efficiently for both sensing and communication. It comprises a monostatic Multiple-Input Multiple-Output (MIMO) radar that transmits precoded OFDM waveforms from its antennas. Unlike previous OFDM DFRC methods, the proposed scheme makes the subcarriers available to multiple antennas in each channel use. We will refer to the proposed system as DFRC with Shared-Subcarriers (DFRC-SS), with the name denoting the shared use of subcarriers by transmit antennas. Subcarrier sharing enables high communication rate. However, it creates two challenges, i.e., (i) at the receiver, on the shared subcarriers, the radar target parameters and the transmitted communication symbols from multiple antennas are coupled, which complicates the target estimation task, and (ii) on the shared subcarriers, the waveforms of the transmit antennas are no longer orthogonal, and thus are not easily separable at the radar receiver, which prevents the formation of a virtual array; the virtual array is a key feature of MIMO radar for achieving high angular resolution [36].

To address the first challenge, one could extract the radar parameters using a maximum likelihood (ML) approach, as that used in MIMO radar [50], where the target parameters are computed by searching over the entire target angle-range-velocity parameter space. However, such an approach would involve high complexity. In this paper, we propose a novel, suboptimal but computationally efficient approach to untangle the radar parameters from the received target echoes on all subcarriers. To address the second challenge, we propose a novel way for the system to enjoy the benefits of a virtual array by controlling the access of transmit antennas to subcarriers. In particular, we propose to set aside a small group of subcarriers, over which, transmit antennas cannot overlap. We will refer to those subcarriers as *private*. By increasing the number of private subcarriers we reduce the communication rate and improve the sensing performance. The improvement is achieved because, based on the signal received on the private subcarriers, and also the target parameter estimates obtained on all subcarriers, a virtual array can be constructed that enables refinement of the target parameter estimates. The private subcarriers could also be used to transmit pilots for channel estimation.

In this work, the precoding matrix is optimally designed to maximize a weighted combination of the DFRC beampattern performance and the communication signal-to-noise (SNR) ratio. This joint design is inspired by the design of [33] but it is modified to address the multicarrier signal scenario, and also the way in which the precoder is applied to the transmit waveforms.

The communication component of the proposed system is along the lines of standard multi-antenna OFDM communications [51], [52], except that the indices of the private subcarriers need to be either estimated by the receiver or encoded into data symbols and transmitted to the receiver in advance.

Our proposed work falls under the joint design category of DFRC methods, except that in addition to using a precoder, it allows one to trade-off communication and sensing performance by controlling the access of transmit antennas to subcarriers. The proposed work can be summarized as follows:

1) A novel DFRC system, referred to as DFRC-SS, is proposed, that transmits OFDM waveforms, where the subcarriers are marked as shared or private. The proposed system makes efficient use of the available bandwidth for communication and sensing by allowing antennas to simultaneously transmit on all shared subcarriers. The private subcarriers are made available to the transmit antennas to transmit in an exclusive fashion.
2) A novel, low-complexity approach is proposed for estimating the radar parameters, which overcomes the coupling of parameters and transmitted symbols arising on the shared subcarriers at the receive antennas. The obtained parameters can then be fine-tuned by constructing a virtual array based on the signals received on the private subcarriers.
3) The proposed DFRC-SS flexibly trades off communication rate for improved target estimation performance by controlling the number of private subcarriers. The system can be configured for maximum communication rate by allocating all subcarriers to transmit antennas as shared, or can trade off communication rate for improved sensing performance by allocating a small number of subcarriers as private.

Preliminary results of this work were reported in [16]. In addition to [16], here, we (i) further exploit the frequency diversity

for angle estimation on the receive array, (ii) explore the trade-off between sensing and communication, (iii) propose ways to further reduce the complexity of target parameter estimation, (iv) introduce precoding for beamforming purposes.

The remainder of this paper is organized as follows. In Section II, we describe the target estimation and communication process using precoded OFDM radar when all subcarriers are used as shared. In Section III, we introduce the use of private subcarriers in addition to shared subcarriers, which trades off the communication rate for improved sensing performance. The communication on private subcarriers is also discussed in Section III. In Section IV, we formulate the precoder design problem. In Section V, we summarize the proposed DFRC-SS system that uses shared and private subcarriers. We provide simulation results on the system performance in Section VI and concluding remarks in Section VII.

Notation: Throughout this paper, we use $\mathbb{R}$ and $\mathbb{C}$ to denote the sets of real and complex numbers, respectively. $(\cdot)^T$ stands for the transposition operator, $(\cdot)^*$ denotes complex conjugate and $(\cdot)^H$ denotes complex conjugate transpose. $||\cdot||_2$ represents ℓ_2 norms. $\lfloor\cdot\rfloor$ denotes the floor function.

II. DFRC-SS With All Subcarriers Used as Shared

Let us consider a *monostatic*, fully digital MIMO radar, comprising an N_t-antenna uniform linear array (ULA) to transmit, and an N_r-antenna ULA to receive. The transmit and receive antenna spacing are g_t and g_r, respectively. The radar transmits precoded OFDM waveforms using N_s subcarriers. All subcarriers are used as *shared*, i.e., they are available to all antennas to transmit simultaneously. The binary source data are divided into N_t parallel streams, one for each transmit antenna, and each stream is modulated via phase shift keying (PSK) or quadrature amplitude modulation (QAM) and distributed to the OFDM subcarriers. The outputs of all streams are processed by a precoding matrix $\mathbf{P}$. An inverse discrete Fourier transform (IDFT) is applied to the data symbols of each stream, a cyclic prefix (CP) is pre-appended to the result, the samples are converted into an analog multicarrier signal with carrier frequency f_c and are transmitted through the corresponding antenna. The transmitted multicarrier signal will be referred to as OFDM symbol.

Let $\mathbf{D}_\mu \in \mathbb{C}^{N_t \times N_s}$ denote a matrix that contains the precoded symbols to be transmitted during the μ-th OFDM symbol, i.e.,

$$\mathbf{D}_\mu = \begin{bmatrix} d(0,0,\mu) & \dots & d(0,N_s-1,\mu) \\ d(1,0,\mu) & \dots & d(1,N_s-1,\mu) \\ \dots & \dots & \dots \\ d(N_t-1,0,\mu) & \dots & d(N_t-1,N_s-1,\mu) \end{bmatrix}, \quad (1)$$

where $d(n,i,\mu)$ denotes the symbol transmitted by the n-th antenna, on the i-th subcarrier, during the μ-th OFDM symbol. The i-th column of $\mathbf{D}_\mu$ contains the symbols transmitted by all antennas on subcarrier i, while the j-th row of $\mathbf{D}_\mu$ contains the symbols transmitted by the j-th antenna on all subcarriers. In the following, for notational simplicity, the use of the symbol matrix will refer to one OFDM symbol. Then the subscript μ will be dropped in $\mathbf{D}_\mu$.

Let $\mathbf{P} \in \mathbb{C}^{N_t \times N_t}$ denote the precoding matrix and $\mathbf{Q} \in \mathbb{C}^{N_t \times N_s}$ the matrix containing the data symbols in each OFDM symbol before precoding. Then,

$$\mathbf{D} = \mathbf{PQ}. \quad (2)$$

The precoding scheme enables beamforming and the precoding matrix, $\mathbf{P}$, will be optimally designed to meet a certain performance metric.

The complex envelope of the baseband signal on the i-th subcarrier transmitted by the n-th antenna equals

$$x(n,i,t) = \sum_{\mu=0}^{N_p-1} d(n,i,\mu) e^{j2\pi i \Delta f t} rect\left(\frac{t-\mu T_p}{T_p}\right), \quad (3)$$

for $n = 1,\dots,N_t$ and $i = 0,1,\dots,N_s-1$, where $rect(t/T_p)$ denotes a rectangular pulse of duration T_p, and Δf is the subcarrier spacing, for which it holds that $\Delta f = 1/(T_p - T_{cp})$ and T_{cp} is the duration of CP.

In the following we make certain assumptions: (1) the length of CP is larger than the maximum between the roundtrip delay to the target and the communication channel length; (2) secondary reflections from the target are attenuated and only contribute noise at the receiver; (3) the duration of the OFDM symbol is small enough to assume that the target range is constant over N_p OFDM symbols; (4) the Doppler frequency induced by the target is assumed to be constant over N_p OFDM symbols; (5) the channel scattering coefficients remain constant during N_p OFDM symbols.

Assumption 1 is required to avoid inter-symbol interference during demodulation and is typical in OFDM systems. Assumption 2 is consistent with high frequencies, which experience high attenuation. Assumptions 3, 4 and 5 depend on N_p, the OFDM parameters and the target radial velocity. As an example, consider the 5G New Radio (NR) high-frequency standard, where one OFDM symbol has a duration of $8.92\,\mu$s [53]. For a target moving with a radial velocity of $100\,\mathrm{m/s}$, during $N_p = 256$ symbols, i.e., during $2.28\,\mathrm{ms}$, the target range changes by 0.228 m only. So we can assume that the range remains approximately constant during 256 symbols. It is also reasonable to assume that the target velocity and the channel scattering characteristics do not change significantly during that time.

Suppose that there are K point targets in the far field, each characterized by angle θ_k, range R_k, and radial velocity v_k. The baseband equivalent of the signal received by the m-th receive antenna on the i-th subcarrier is

$$y(m,i,t) = \sum_{k=1}^{K}\sum_{n=1}^{N_t} \beta_k x(n,i,t-\tau_{kmn}) e^{j2\pi f_{d_k}^i t} + u_i(m,t), \quad (4)$$

for $m = 0,\dots,N_r-1$, where β_k is a complex coefficient accounting for the scattering process associated with the k-th target; $f_{d_k}^i$ is the Doppler frequency of the k-th target, which is equal to

$$f_{d_k}^i = 2v_k(f_c + i\Delta f)/c, \quad (5)$$

with c denoting the speed of light;

$$\tau_{kmn} = [2R_k + (ng_t + mg_r)\sin\theta_k]/c,$$

is the roundtrip delay of the k-th target, and $u_i(m,t)$ denotes independent and identically distributed (i.i.d.) white Gaussian noise with zero mean and variance σ_r^2, or clutter. Based on assumption 3, the roundtrip delay is taken as constant during the OFDM symbol interval. The coefficients β_k depend on the target only [54], [55], and due to assumption 5, they are constant over N_p OFDM symbols. Those coefficients do not need to be known, and as we will discuss in Section III-A, can actually be estimated during the sensing process.

In the received target echoes (see (4)), the radar target parameters and the transmitted communication symbols from multiple antennas are coupled, which complicates the target estimation task. Next we introduce a low-complexity approach to decouple and estimate the radar parameters.

A. Target Angle Estimation

For simplicity, the rectangular pulse function and CP will be omitted in the following formulations. The received signal on the i-th subcarrier during the μ-th OFDM symbol duration can be expressed as

$$y(m,i,t) = \sum_{k=1}^{K} e^{-j2\pi m g_r \sin\theta_k \frac{f_c+i\Delta f}{c}} \times \sum_{n=1}^{N_t} \beta_k d(n,i,\mu) e^{-j2\pi n g_t \sin\theta_k \frac{f_c+i\Delta f}{c}} \times e^{-j2\pi i\Delta f \frac{2R_k}{c}} e^{j2\pi f_{d_k}^i t} e^{j2\pi i\Delta f t} + u_i(m,t). \quad (6)$$

Let us express continuous time t as $t = \mu T_p + \tau$, where $\tau \in [0, T_p)$. As done in typical OFDM demodulation, the receiver first samples $y(m,i,t)$ in time with sampling frequency $F_s = \Delta f \times N_s$, over duration $T_p - T_{cp}$ [8]. The sample index corresponding to the sampling of τ is usually referred to as *fast time*, while the OFDM symbol index, μ, is referred to as *slow time*. By applying an N_s-point DFT on the obtained samples, the fast time domain is transformed to the index of subcarriers, and the receiver obtains the modulated symbol which was transmitted on each subcarrier. The symbol received by the m-th receive antenna on the i-th subcarrier equals

$$d_r(m,i,\mu) = \sum_{k=1}^{K}\sum_{n=1}^{N_t} \beta_k d(n,i,\mu) e^{-j2\pi(m g_r + n g_t)\sin\theta_k \frac{f_c+i\Delta f}{c}} \times e^{-j2\pi i\Delta f \frac{2R_k}{c}} e^{j2\pi\mu T_p f_{d_k}^i} + U(m,i,\mu), \quad (7)$$

where $U(m,i,\mu)$ denotes the N_s-point DFT of the noise during the μ-th OFDM symbol. (7) can be viewed as

$$d_r(m,i,\mu) = \sum_{k=1}^{K} A(k,i,\mu) e^{j2\pi\omega(k,i)m} + U(m,i,\mu), \quad (8)$$

for $m = 0, \ldots, N_r - 1$, where

$$A(k,i,\mu) = \sum_{n=1}^{N_t} \beta_k d(n,i,\mu) e^{-j2\pi n g_t \sin\theta_k \frac{f_c+i\Delta f}{c}} \times e^{-j2\pi i\Delta f \frac{2R_k}{c}} e^{j2\pi\mu T_p f_{d_k}^i}, \quad (9)$$

and

$$\omega(k,i) = -g_r \sin\theta_k \frac{f_c + i\Delta f}{c}. \quad (10)$$

The symbols $d(n,i,\mu)$ are known to the radar receiver as this is a monostatic radar.

Let us assume that $N_r > K$. For a fixed i and μ, based on (8), the sequence $\{d_r(m,i,\mu), m = 0, \ldots, N_r - 1\}$ can be viewed as a sum of K complex sinusoids with spatial frequencies $\omega(k,i)$ and complex amplitudes $A(k,i,\mu)$. Thus, upon applying an N_r-point DFT on that sequence, we find peaks at frequencies $\omega(k,i)$ (see Fig. 1). Once the $\omega(k,i)$ are estimated, the target angles can be computed as

$$\theta_k = \arcsin\left(-\frac{\omega(k,i)c}{g_r(f_c + i\Delta f)}\right). \quad (11)$$

The angle estimation scheme can be repeated on all subcarriers. Thus, by exploiting frequency diversity, one can find all occupied angle bins with high probability.

The resolution of the peaks in the aforementioned DFT depends on the number of receive antennas, N_r. We will refer to the angle estimates of (11) as *coarse*, and in Section III-A, we will show how these angles estimates can be refined.

We should note that in the above estimation, the complex amplitude β_k does not need to be known, because the coarse angle estimation is along the receive array domain.

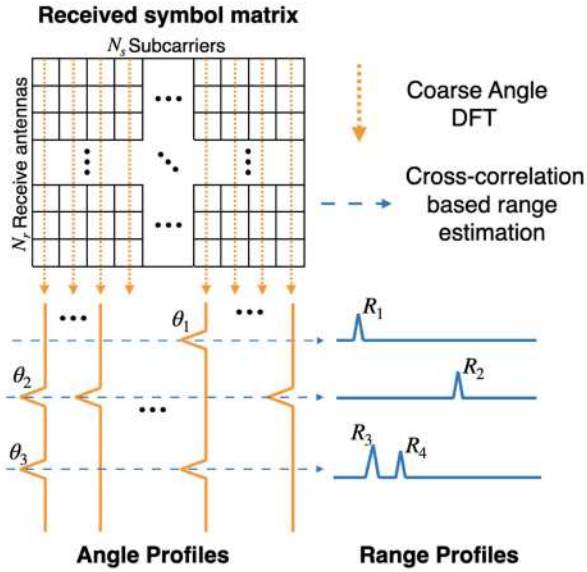

Fig. 1. Estimation of angle and range in one OFDM symbol.

B. Range Estimation

One way to extract the target range-Doppler parameters would be via the maximum likelihood estimation approach used in MIMO radar [50]. This would amount to cross-correlating the received signal at each possible range-Doppler bin with the transmitted symbols and finding the range-Doppler bin that maximizes the output. However, such an approach involves high

complexity and also suffers from convergence and resolution problems [56]. Here, we propose a suboptimal but computationally simpler estimation approach as follows.

The amplitudes corresponding to frequencies $\omega(k,i)$, given in (9), contain known precoded symbols, estimated target angles, and unknown ranges and Doppler frequencies. Inside each occupied angular bin, there may be multiple targets. Suppose that there are N_k targets corresponding to the k-th estimated direction θ_k. Then, the corresponding amplitude can be expressed as

$$\begin{aligned} A(k,i,\mu) &= \sum_{n=1}^{N_t} d(n,i,\mu) e^{-j2\pi n g_t \sin\theta_k \frac{f_c+i\Delta f}{c}} \\ &\quad \times \sum_{q=1}^{N_k} \beta_{kq} e^{-j2\pi i \Delta f \frac{2R_q}{c}} e^{j2\pi\mu T_p f_{d_q}^i}, \\ &= A'(k,i,\mu) \sum_{q=1}^{N_k} \beta_{kq} e^{-j2\pi i \Delta f \frac{2R_q}{c}} e^{j2\pi\mu T_p f_{d_q}^i}, \end{aligned} \tag{12}$$

where β_{kq} is the coefficient of the q-th target at angle θ_k and

$$A'(k,i,\mu) = \sum_{n=1}^{N_t} d(n,i,\mu) e^{-j2\pi n g_t \sin\theta_k \frac{f_c+i\Delta f}{c}}. \tag{13}$$

Based on (5), (12) can be written as

$$A(k,i,\mu) = A'(k,i,\mu) \sum_{q=1}^{N_k} \beta_{kq} e^{j2\pi\mu T_p \frac{2v_q f_c}{c}} e^{j2\pi i \omega_r(q,\mu)}, \tag{14}$$

where

$$\omega_r(q,\mu) = -2\Delta f \frac{R_q - \mu T_p v_q}{c}. \tag{15}$$

Due to assumption 3, the term $\mu T_p v_q$ is significantly smaller that R_q, thus $\omega_r(q,\mu)$ could be simplified as

$$\omega_r(q) \approx -\Delta f \frac{2R_q}{c}. \tag{16}$$

This simplification implies that the range term in (14) changes along the fast time only, and the radial velocity term changes along the slow time only. Thus, the two quantities can be independently estimated.

In (14), $A'(k,i,\mu)$ contains known symbols and angles that have been already estimated. One could divide $A(k,i,\mu)$ by $A'(k,i,\mu)$ and then compute range and Doppler by taking DFT across i and μ, respectively. However, the division may lead to problems when the denominator is close to zero. Instead of division, we propose the following approach to estimate range and Doppler.

Let $\mathcal{A}(k,\ell,\mu)$ and $\mathcal{A}'(k,\ell,\mu)$ denote respectively the N_s-point DFT of $A(k,i,\mu)$ and $A'(k,i,\mu)$ along dimension i. One can see that $\mathcal{A}(k,\ell,\mu)$ is a weighted sum of shifted versions of $\mathcal{A}'(k,\ell,\mu)$, with shifts equal to $\omega_r(q)$ and weights equal to $\beta_q e^{j2\pi\mu T_p \frac{2v_q f_c}{c}}$. Since $A'(k,i,\mu)$ has already been estimated, the shifts $\omega_r(q)$ can be measured based on the locations of the peaks in the cross-correlation of $\mathcal{A}'(k,\ell,\mu)$ and $\mathcal{A}(k,\ell,\mu)$ (see Fig. 1). The peaks appear at indices

$$l_q = \left\lfloor \frac{2N_s R_q \Delta f}{c} \right\rfloor, \tag{17}$$

revealing the ranges of the targets that fall in angle bin θ_k, i.e., $R_q, q = 1,\ldots,N_k$.

The resolution of range estimates is

$$R_{res} = \frac{c}{2N_s\Delta f} = \frac{c}{2B}, \tag{18}$$

where B is the bandwidth of the OFDM waveforms, and the maximum detectable range is

$$R_{\max} = \frac{c}{2\Delta f}. \tag{19}$$

Based on (19), for a large unambiguous range the subcarrier spacing should be as small as possible. On the other hand, since the OFDM symbol duration equals $T_p = \frac{1}{\Delta f} + T_{cp}$, a small subcarrier spacing results in a longer OFDM symbol duration.

We should note that the obtained range estimates use the full available bandwidth, and thus have the maximum possible resolution. However, range estimation will be affected by errors in angle estimation. If due to low angle resolution some angles are missed, the corresponding ranges may be missed. Later, in Section III-A, we will discuss how we can correct this potential problem by trading off communication rate for improved sensing performance.

C. Doppler Estimation

For each estimated range, the corresponding Doppler frequency can be estimated by taking an N_p-point DFT of the cross-correlation peak values, i.e., $\beta_q e^{j2\pi\mu T_p \frac{2v_q f_c}{c}}$, corresponding to N_p OFDM symbols, i.e., for $\mu = 1,\ldots,N_p$. The DFT will contain peaks at indices

$$p_q = \lfloor N_p T_p f_{d_q}^0 \rfloor = \left\lfloor \frac{2v_q f_c N_p T_p}{c} \right\rfloor, \tag{20}$$

which provide the targets' Doppler frequencies and thus their velocities. By estimating the Doppler parameter for each range peak, we can match the Doppler estimates with the estimated ranges. Since the target ranges are estimated within certain angle bins, and the Doppler frequencies are estimated based on each range peak (see Fig. 1), the angle-range-Doppler parameters of a given target are paired together. Again, the complex amplitudes β_q do not need to be known, and they can actually be estimated based on the values of Doppler DFT peaks.

The resolution of the target velocity estimation and maximum detectable velocity are

$$v_{res} = \frac{c}{2f_c N_p T_p}, \tag{21}$$

$$v_{\max} = \frac{c}{2f_c T_p}, \tag{22}$$

respectively. Note that the radial velocities could be both positive and negative, thus the maximum unambiguous velocity is half of the detectable velocity.

From (22), an increased T_p will reduce the detectable velocity. In real world systems, the subcarrier spacing needs to be chosen

carefully paying attention to the trade-off between the maximum unambiguous range and the maximum detectable velocity.

D. The Communication Component

Let us consider the communication component of the proposed DFRC-SS system when all subcarriers are used as shared. Suppose there is a multi-antenna receiver, with N_c antennas, spaced apart by d_r, that can perform OFDM demodulation. We assume that $N_c > N_t$ and the receiver knows the type of constellation used by the transmitter and also the precoding matrix that has been used. We also assume that the receiver can estimate the communication channel via pilots. The above assumptions are typical in precoded OFDM communication systems.

Due to the narrow bandwidth of each subcarrier, the signals on each subcarrier experience flat fading. The symbols across all receive antennas can be expressed as

$$\mathbf{r}_i = \mathbf{H}_i \mathbf{d}_i + \mathbf{u}_i,\ i = 0, \ldots, N_s - 1, \tag{23}$$

where i is the subcarrier index, $\mathbf{H}_i \in \mathbb{C}^{N_c \times N_t}$ is the channel matrix on the i-th subcarrier, $\mathbf{d}_i$ is the i-th column of $\mathbf{D}$, and $\mathbf{u}_i \in \mathbb{C}^{N_c \times 1}$ represents the measurement noise on the i-th subcarrier; the noise is assumed to be white, Gaussian with zero mean and covariance $\sigma_c^2 \mathbf{I}$.

The data symbol vector can be estimated via least-squares, i.e.,

$$\arg\min_{\mathbf{q}} ||\mathbf{r}_i - \mathbf{H}_i \mathbf{P} \mathbf{q}||_2^2. \tag{24}$$

By applying the same process to every subcarrier and every received OFDM symbol, all transmitted symbols can be estimated. Compared with an OFDM communication system with the same modulation scheme but without subcarrier sharing, the proposed system increases the number of information bits transmitted in one period by a factor of N_t.

III. Trading Off Communication Rate for Target Estimation Performance Using Private Subcarriers

In the above described system, where all subcarriers are shared, angle estimation relies on the aperture of the physical array, i.e., $(N_r - 1)g_r$. As a result, angle resolution is limited by the size of the receive array. Low angle resolution may render some target angles unresolvable. Since the angle estimates are used to obtain target range and Doppler, angle estimation errors will propagate to those parameters as well. In this section, we introduce the use of *private* subcarriers, and show how they can be used to construct a virtual array, which can improve the coarse target angle estimates.

A private subcarrier is uniquely paired with a transmit antenna, and thus carries the symbols of that antenna only. Let us assume that M out of the N_s subcarriers are allocated as private, where $1 \leq M \leq N_t$, and let $\mathcal{M}$ denote the set of private subcarrier indices. Private subcarrier i is uniquely assigned to transmit antenna n_i. The remaining $N_s - M$ subcarriers are assigned to transmit antennas in a shared fashion. Let $\tilde{\mathbf{Q}} \in \mathbb{C}^{N_t \times N_s}$ be the symbol matrix before precoding in this shared-private subcarrier case. Its columns $\tilde{\mathbf{q}}_i, i \in \mathcal{M}$ contain all zeros except one non-zero element at position n_i, corresponding to the symbol $q(n_i, i, \mu)$ placed by antenna n_i on that subcarrier. All other columns of $\tilde{\mathbf{Q}}$ are identical to those of $\mathbf{Q}$ in (2). For simplicity, here we let $\mathcal{M} = \{0, 1, \ldots, M-1\}$ and set $n_i = i$. In general, the set $\mathcal{M}$ could contain any subcarriers, and its composition can change between OFDM symbols. Also the indices of transmit antennas corresponding to the private subcarriers can change between OFDM symbols.

Let there be no precoding on the private subcarriers. In other words, the transmitted symbols on subcarrier i are $\mathbf{d}_i = \mathbf{P}\mathbf{q}_i$ if $i \notin \mathcal{M}$, and $\mathbf{d}_i = \tilde{\mathbf{q}}_i$ if $i \in \mathcal{M}$. By doing so, the waveforms transmitted by the antennas over the private subcarriers are orthogonal, which ensures that they can be separated at the receiver. In order to keep the same power level on private subcarriers as on the shared ones, $q(n_i, i, \mu)$ is appropriately scaled to have power γ^2.

From (7), omitting the noise term and performing element-wise division by the known symbol $q(n_i, i, \mu)$, the received symbol on the same subcarrier becomes

$$d_r'(m, i, \mu) = \sum_{k=1}^{K} \beta_k e^{-j2\pi(m g_r + n_i g_t)\frac{\sin\theta_k}{\lambda_i}} \times e^{-j2\pi i \Delta f \frac{2R_k}{c}} e^{j2\pi\mu T_p f_{d_k}^i}, \quad i \in \mathcal{M}. \tag{25}$$

with λ_i denoting the wavelength of the i-th subcarrier.

Let us define the transmit and receive steering vectors corresponding to the i-th subcarrier as

$$\mathbf{a}_r(\theta, i) = [1, e^{-j2\pi g_r \frac{\sin\theta}{\lambda_i}}, \ldots, e^{-j2\pi(N_r-1)g_r\frac{\sin\theta}{\lambda_i}}]^T, \tag{26}$$

$$\mathbf{a}_t(\theta, i) = [1, e^{-j2\pi g_t \frac{\sin\theta}{\lambda_i}}, \ldots, e^{-j2\pi(N_t-1)g_t\frac{\sin\theta}{\lambda_i}}]^T, \tag{27}$$

respectively, where $\lambda_i = \frac{f_c + i\Delta f}{c}$.

By stacking the symbols (see (25)) received by all antennas on private subcarrier i in a column vector, i.e., $\mathbf{z}_i \in \mathbb{C}^{N_r \times 1}$, we have that

$$\mathbf{z}_i = \sum_{k=1}^{K} \beta_k e^{j2\pi\mu T_p f_{d_k}^i} e^{-j2\pi n_i g_t \frac{\sin\theta_k}{\lambda_i}} e^{-j2\pi i \Delta f \frac{2R_k}{c}} \mathbf{a}_r(\theta_k, i). \tag{28}$$

By further stacking the resulting vectors from all private subcarriers into a long vector, i.e., $\mathbf{z} = [\mathbf{z}_0^T, \ldots, \mathbf{z}_{M-1}^T]$, based on (28) and using the approximation of (16), we can write

$$\mathbf{z} = \sum_{k=1}^{K} \beta_k e^{j2\pi\mu T_p f_{d_k}^0} \mathrm{vec}\{\mathbf{A}_r(\theta_k)\mathrm{diag}[\tilde{\mathbf{a}}_t(\theta_k, R_k)]\}, \tag{29}$$

where $\mathrm{vec}\{\cdot\}$ is the vectorization operator,

$$\mathbf{A}_r(\theta_k) = [\mathbf{a}_r(\theta_k, 0), \ldots, \mathbf{a}_r(\theta_k, M-1)], \tag{30}$$

$$\tilde{\mathbf{a}}_t(\theta_k, R_k) = \mathbf{a}_t^p(\theta_k) \odot \mathbf{b}(R_k), \tag{31}$$

with $\odot$ denoting Hadamard product,

$$\mathbf{b}(R_k) = [1, e^{-j2\pi\Delta f \frac{2R_k}{c}}, \ldots, e^{-j2\pi(M-1)\Delta f \frac{2R_k}{c}}]^T, \tag{32}$$

and

$$\mathbf{a}_t^p(\theta) = [1, e^{-j2\pi g_t \frac{\sin\theta}{\lambda_1}}, \ldots, e^{-j2\pi(M-1)g_t\frac{\sin\theta}{\lambda_{M-1}}}]^T. \tag{33}$$

In the above expression, z can be effectively viewed as the response of a virtual array (VA) [57]. The VA has an aperture that is M times larger than the aperture of the physical receive array, and thus can enable better angle resolution. Unlike typical VAs, however, its steering vector, i.e., $\text{vec}\{\mathbf{A}_r(\theta_k)\text{diag}[\tilde{\mathbf{a}}_t(\theta_k, R_k)]\}$, depends on target range as well as angle, and also on the private subcarrier set $\mathcal{M}$ and the corresponding transmit antenna set.

A. Refining the Angle Estimates

The target parameter estimation method proposed in Section II still holds if some subcarriers are private. This is because coarse angle estimation is along the receive array, which is independent of the data symbols. Also, range estimation is based on (13), which is the summation over all modulated data symbols on the i-th subcarrier. Thus, range estimation holds for both private and shared subcarriers. Doppler estimation based on the range peaks also holds on both private and shared subcarriers.

Suppose that we have obtained coarse angles estimates and the corresponding ranges $\{R_1, R_2, \ldots, R_N\}$ based on all (shared and private) subcarriers using the method of Section II. In the following, we describe how those estimates can be refined by formulating and solving a reduced dimensionality sparse signal recovery (SSR) problem.

Let us discretize the angle space around the coarse angle estimates, taking N_a grid points. Then, (29) can be expressed as

$$\begin{aligned}\mathbf{z} &= [\mathbf{z}_{11}, \mathbf{z}_{12}, \ldots, \mathbf{z}_{N_a N}] \begin{bmatrix} \tilde{\beta}_{11}, \\ \ldots, \\ \tilde{\beta}_{N_a N} \end{bmatrix}, \\ &= [\mathbf{z}_{11}, \mathbf{z}_{12}, \ldots, \mathbf{z}_{N_a N}]\tilde{\beta}, \end{aligned} \tag{34}$$

where $\tilde{\beta}_{ij}$ is non zero if there is a target at range R_j and angle grid point $\tilde{\theta}_i$, and

$$\mathbf{z}_{ij} = \text{vec}\{\mathbf{A}_r(\tilde{\theta}_i)\text{diag}[\mathbf{a}_t^p(\tilde{\theta}_i) \odot \mathbf{b}(R_j)]\}, \tag{35}$$

is the dictionary element for $i = 1, 2, \ldots, N_a$ and $j = 1, 2, \ldots, N$. Assuming that the target angle-range space around the considered regions is sparse, thus vector $\tilde{\beta}$ is sparse which can be estimated under certain conditions [58] via ℓ_1-norm minimization [59]. The support of $\tilde{\beta}$ provides the angle-range space grid points that are the closest to the target angles. We should note that, upon using the previously estimated ranges to construct the base matrix, the refined angle estimates are naturally paired with those range estimates.

The natural question is now whether we should trust the ranges obtained based on the coarse angle estimates, and rely on them to construct the problem of (34). When using all (private and shared) subcarriers, the range estimates obtained from (17) use all the available bandwidth, and thus have the maximum possible resolution. So, further discretization of the range space around those estimates would not help the basis matrix of (34). However, there can be cases in which some angles maybe not be resolvable, or can be missed. For example, due to low angle resolution, some angles may not be resolvable and will appear in the same bin. In that case, the corresponding ranges will all appear inside that angle bin. Also, if there is not enough frequency diversity (i.e., not enough subcarriers) to obtain good coarse angle estimates, it is possible that some target angles maybe be missed, causing the corresponding ranges to be missed. Of course, such a case would not arise in wideband OFDM systems with a large number of subcarriers. Also, if in (7), it holds that for some k, $A(k, i, \mu) \approx 0$ for all subcarriers i, (this of course would happen with a small probability), then the corresponding spatial frequency and associated ranges will be missed.

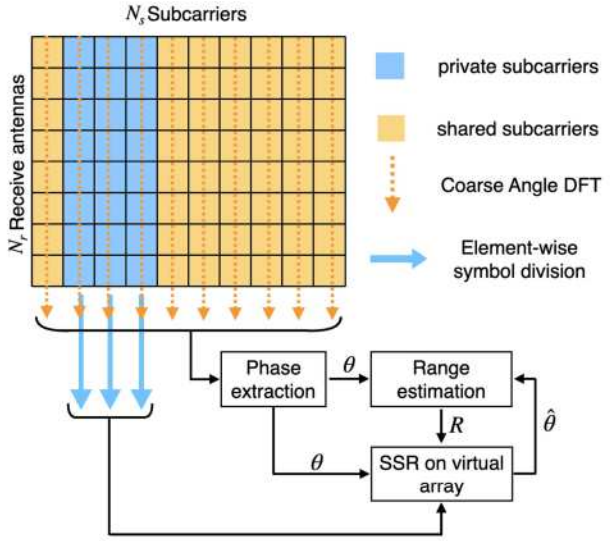

Fig. 2. Target estimation with private subcarriers in an SS-OFDM DFRC system.

Based on extensive experience with simulations, in those rare cases, the SSR problem formulated based on the obtained coarse angle estimates and corresponding ranges will still yield refined angle estimates and reveal the missed target angles. Based on the new angles we can revisit (17) to compute the corresponding ranges.

The entire estimation process is illustrated in Fig. 2. The obtained refined estimates can be used in (12) to obtain Doppler estimates. In Fig. 2, solving the SSR problem has a dominant complexity, which depends on the size of the base matrix (see (34)).

We should note that the angle-range estimation is done using one OFDM symbol only, while Doppler estimation requires N_p OFDM symbols and is carried out in the slow time domain. After Doppler estimation, the coefficient β_k can be computed based on the nonzero elements of $\tilde{\beta}$.

Remark 1: The formulated virtual array, unlike the conventional virtual array, depends not only on the target angle but also on the target range, private subcarrier indices and the corresponding transmit antenna indices. Although the target angle and range are assumed to be constant between OFDM symbols, different pairings of private subcarriers and transmit antennas provide frequency and spatial diversity, which can be exploited to improve target estimation.

Remark 2: As the proposed system is wideband, the resolution of range estimation is high. Thus, in order to reduce the computational complexity and thus save computation time

and overhead, we chose not to discretize the range space and directly use the range estimates corresponding to the coarse angle estimates to formulate the SSR problem. However, if the bandwidth is not large, one can discretize range space as well.

Remark 3: One may argue that the SSR problem could be constructed without using the coarse angle and corresponding range estimates, by discretizing the entire target space and forming an overcomplete problem for both range and angle estimation. However, such an approach would have the following shortcomings. First, the entire range and angle space most probably will not be sparse enough for SSR to work well; sparseness can be assumed only within small angle-range space regions. Second, such an approach would result in a high-dimensional SSR problem, which takes a long time to solve.

The proposed estimation approach bears some similarity to the method of [60] proposed for resolving the range ambiguity problem in a frequency diverse array (FDA) radar with angle-range dependent virtual array, arising when the frequency of the waveform is increased with a small amount across the array elements, although our scenario faces more complicated coupling due to the transmitted data symbols. Both methods first coarsely estimate the target parameters and then use the results to refine estimation. The difference is that here we use the entire virtual array to estimate angle, thus enjoying higher resolution, while [60] uses the receive array only. Also, our formulated virtual array depends on the locations of private subcarriers and the corresponding antenna indices, where the frequency and spatial diversity could be exploited. Our method can recover targets unresolved in the coarse estimation, and the range estimates that we use for angle estimation are always at maximum resolution. Thus the results of our method are refined angle and range estimates, while the result in [60] are only refined range estimates.

B. Communication on Private Subcarriers

OFDM communication systems transmit pilots over certain subcarriers, so that the receiver can estimate the channel. The private subcarriers can actually be used to transmit pilot symbols for channel estimation. Since the set of private subcarriers can be any subset of cardinality M of the available subcarriers, and they can be paired with any set of transmit antennas, by changing the private subcarriers subset and the corresponding transmit antennas between OFDM symbols, one can obtain samples of the channel frequency response. The rest of the channel frequency response can then be obtained via interpolation [61]. To have good channel estimation, one should use subcarriers with good SNR as private subcarriers. In that case, the communication receiver would need to first identify the private subcarriers and also the active antennas on those subcarriers. For that purpose, the receiver can leverage the fact that the transmitted data symbol vector on the private subcarriers is naturally 1-sparse, while the data symbol vector on the shared subcarriers has mostly nonzero entries. Thus, the private subcarriers can be identified by solving a least-squares problem on each subcarrier, and then checking for 1-sparseness in the result. The support of the sparse vector yields the index of the active antenna.

The complexity of symbol decoding and private subcarrier detection is given in Section V-A. To avoid the latency associated with the detection of private subcarriers, the locations of the private subcarriers and the pairing between transmit antennas during the μ-th OFDM symbol can be encoded in the $(\mu-1)$-th OFDM symbol, so that the communication receiver has the information when needed. To encode the locations of M private subcarriers and the pairing between transmit antennas in the next OFDM symbol, the number of required bits is

$$\left\lceil \log_2 \frac{N_s!}{(N_s-M)!} \right\rceil, \tag{36}$$

where $\lceil\cdot\rceil$ denotes the ceiling function. (36) accounts for the permutation of M private subcarriers in total N_s subcarriers.

C. Communication Rate and Sensing Performance Trade-Off

The use of private subcarriers improves the sensing performance, but results in a rate loss of $\epsilon = \frac{M}{N_s}(\%)$. When $M=0$, the system achieves the maximum communication rate. By increasing M, we can flexibly trade-off bit rate for improved sensing performance. As it will be seen in the simulations section, in a wideband OFDM system with a large number of subcarriers, the loss from private subcarriers is small as the needed M is typically much smaller than N_s.

The use of private subcarriers does not only benefit the radar. The private subcarriers could also be used to estimate the communication channels by transmitting pilot symbols on them. The selection of private subcarriers, and the pairing of private subcarriers with transmit antennas can also be used to encode information and thus partially compensate for the communication rate loss incurred by the use of private subcarriers. This was investigated in our previous work [62] where we also proposed a low-complexity binary search method to identify the private subcarriers at the receiver side.

IV. Precoder Design

The precoder is obtained by optimizing a weighted combination of beampattern error and the average SNR on all subcarriers at the communication receiver. Since precoding destroys the orthogonality of the transmitted waveforms, the precoder is applied to the signals to be transmitted on the shared subcarriers only. In that way, the signals on the private subcarriers are orthogonal and can be used to formulate the virtual array.

A. Beampattern Error

Let $\mathbf{F} \in \mathbb{C}^{N_s \times N_s}$ denote the inverse Fourier transform matrix. The baseband transmitted signal corresponding to the μ-th OFDM symbol can be expressed in matrix form as

$$\mathbf{X} = \mathbf{P}\tilde{\mathbf{Q}}\mathbf{F}, \tag{37}$$

where $\tilde{\mathbf{Q}}$ is the symbol matrix as defined in Section III. The j-th column of the baseband signal matrix $\mathbf{X}$, or otherwise, the j-th

snapshot, equals

$$\mathbf{x}_j = \sum_{i=0, i\notin\mathcal{M}}^{N_s-1} \mathbf{P}\mathbf{q}_i F(i,j) + \sum_{i\in\mathcal{M}} \tilde{\mathbf{q}}_i F(i,j), \tag{38}$$

where $F(i,j)$ is the element on the i-th row and j-th column of $\mathbf{F}$. Recall that $\tilde{\mathbf{q}}_i$ is 1-sparse, with its non-zero-element in the n_i-th position and γ^2 is the average power assigned to the symbols transmitted on private subcarriers. The array output towards direction θ at the j-th snapshot is

$$y_j(\theta) = \sum_{i=0, i\notin\mathcal{M}}^{N_s-1} \mathbf{a}_t^T(\theta,i)\mathbf{P}\mathbf{q}_i F(i,j) + \sum_{i\in\mathcal{M}} \mathbf{a}_t^T(\theta,i)\tilde{\mathbf{q}}_i F(i,j), \tag{39}$$

and the transmitted power along angle θ equals

$$\begin{aligned}\hat{p}_j(\theta) &= \mathbb{E}\{y_j(\theta)y_j(\theta)^*\},\\ &= \frac{1}{N_s}\sum_{i=0, i\notin\mathcal{M}}^{N_s-1} \mathbf{a}_t^T(\theta,i)\mathbf{P}\mathbf{R}_i\mathbf{P}^H\mathbf{a}_t^*(\theta,i)\\ &\quad + \frac{1}{N_s}\sum_{i\in\mathcal{M}} \mathbf{a}_t^T(\theta,i)\tilde{\mathbf{R}}_i\mathbf{a}_t^*(\theta,i),\\ &= \frac{1}{N_s}\sum_{i=0, i\notin\mathcal{M}}^{N_s-1} \mathbf{a}_t^T(\theta,i)\mathbf{P}\mathbf{R}_i\mathbf{P}^H\mathbf{a}_t^*(\theta,i)\\ &\quad + \frac{M}{N_s}\gamma^2,\end{aligned} \tag{40}$$

where $F(i,j)F^*(i,j) = (1/N_s)$, $\mathbf{R}_i = E\{\mathbf{q}_i\mathbf{q}_i^H\}$ is the covariance matrix of the i-th original symbol vector $\mathbf{q}_i$ and $\tilde{\mathbf{R}}_i$ is the covariance matrix of $\tilde{\mathbf{q}}_i$. We should note that the second term is independent of angle, i.e., the power of the signal transmitted on the private subcarriers is spread to the entire angle space.

Let $p(\theta)$ be the desired power of the transmitted signal towards direction θ. The beampattern error with respect to the desired beampattern $p(\theta)$, computed on G discrete angles θ_g in $[-\pi/2, \pi/2]$, equals

$$\begin{aligned}&\sum_{g=1}^{G}\gamma_g[p(\theta_g) - \hat{p}(\theta_g)]^2\\ &= \left\|\Gamma\odot\left(\mathbf{p} - \frac{1}{N_s}\sum_{i=0, i\notin\mathcal{M}}^{N_s-1}\mathrm{diag}\{\mathbf{A}_i^T\mathbf{P}\mathbf{R}_i\mathbf{P}^H\mathbf{A}_i^*\} - \frac{M\gamma^2}{N_s}\mathbf{1}_G\right)\right\|_2^2,\end{aligned} \tag{41}$$

where γ_g are weights that control the importance of beampattern error from the g-th angle, $\Gamma = [\gamma_1, \ldots, \gamma_G]^T$, $\mathbf{p} = [p(\theta_1), \ldots, p(\theta_G)]^T$, $\mathbf{A}_i = [\mathbf{a}_t(\theta_1, i), \ldots, \mathbf{a}_t(\theta_G, i)] \in \mathbb{C}^{N_t\times G}$ is the transmit steering matrix on the i-th subcarrier and $\mathbf{1}_G = [1, \ldots, 1]^T \in \mathbb{R}^G$.

B. SNR at the Communication Receiver

From (23), the power of received symbols from all subcarriers in the μ-th OFDM symbol can be expressed as

$$\mathbf{P}_r = \sum_{i=0, i\notin\mathcal{M}}^{N_s-1} tr[\mathbf{H}_i\mathbf{P}\mathbf{R}_i\mathbf{P}^H\mathbf{H}_i^H] + \sum_{i\in\mathcal{M}} tr[\mathbf{H}_i\tilde{\mathbf{R}}_i\mathbf{H}_i^H], \tag{42}$$

where $tr[\cdot]$ refers to the trace of a matrix. Recall that the power of communication noise is σ_c^2, thus the SNR at the communication receiver equals

$$\gamma_{SNR} = \frac{\mathbf{P}_r}{N_s\sigma_c^2}. \tag{43}$$

C. The Sensing-Communications Co-Design Problem

Let us consider the loss function

$$\mathcal{L}(\mathbf{P}) \triangleq \alpha_b\sum_{g=1}^{G}\gamma_g[p(\theta_g) - \hat{p}(\theta_g)]^2 + (1-\alpha_b)10\log_{10}(\gamma_{SNR}), \tag{44}$$

where α_b is the cost parameter reflecting the relative importance of the beampattern error (first term).

By adjusting α_b, one can put more emphasis on approximating the desired beampattern for radar purposes, or on maximizing the SNR for communication purposes.

We should note that the loss function (44) could have negative values due to the SNR term. Thus when implementing the loss function, a constant could be added to the SNR term which means that the SNR loss is computed as the difference between the desired value and the current SNR. The added constant will not change the result since it will not change the gradient of the loss function.

In the experiments, to solve (44) we used the Adam stochastic optimizer [63] with different learning rates, starting at 0.02, and 600 steps of iterations. Note that the learning rates here only relate to the step length. Different learning rates, help us avoid local optima. A large number of executed steps ensures stable convergence.

The above metric is an extension of [33] to the multi-carrier signal case, after taking into account the way in which the precoding matrix is applied to the transmitted signals. Compared to [32], [34], a design that approximates the desired beampattern also provides high SNR and low radar CRB and MI. Moreover, a good beampattern also avoids transmitting energy towards clutter contributing regions.

V. Summary of the Proposed DFRC-SS With Shared and Private Subcarriers

Putting together all the above presented ideas the proposed system is summarized as follows.

Let us assume that channel estimation is conducted by the communication receiver as done in standard OFDM systems [61]. Also, suppose that the communication receiver position is known to the transmitter and the angle space of the potential targets is also known.

Step 1 Depending on the maximum range and velocity, that we wish to achieve, and the minimum communication rate we need to sustain, the OFDM system parameters and the maximum number of private subcarriers (M) are determined. The channel estimates can be used to determine which subcarriers have good SNR to be used as private.

Step 2 The precoding matrix is estimated, ensuring that the radar will probe a certain angle space, say Θ for possible targets, and will also provide a good SNR level to a communication receiver. Then the precoding matrix is communicated to the communication receiver, as done in standard precoded OFDM systems.

Step 3 Subcarrier sharing is enabled and the precoding matrix is applied to the data to be transmitted on the shared subcarriers (see (2)). The communication receiver decodes the original data symbols.

After receiving each OFDM symbol echo signal, coarse angle-DFT along the receive array domain (see (11)) is applied on all subcarriers. For each angle peak, cross-correlation based range estimation (see (17)) is carried out. Subsequently, target angle estimate refinement is performed by using the signal received on the private subcarriers to formulate and solve an SSR problem (see (34)). The solution provides refined and possibly new angles, which are fed back to the cross-correlation based range estimation to uncover any missed ranges. For each detected range peak, cross-correlation based velocity estimation (see (20)) is conducted after N_p OFDM symbols have been received.

A. Complexity

Here, we will analyze the complexities of the proposed sensing method and the corresponding communication processing in the DFRC-SS.

The complexity of coarse angle estimation is $\mathcal{O}(N_r \log N_r)$. Here we assume that the estimation on all N_s subcarriers can be executed in parallel.

In the cross-correlation based range estimation, since the cross-correlation can be computed via DFT operations, the computation complexity of range estimation is $\mathcal{O}(N_s \log N_s)$. Here we assume that the estimation on the K occupied angle bins can be done in parallel. If there is a small number of targets in each angle-range bin, the N_p-point DFT for velocity estimation can be replaced with a sparse Fourier transform (SFT) [64], which offers significantly reduced complexity. For an exact N_k-sparse case, the average complexity of estimating the N_k Doppler frequencies is $\mathcal{O}(N_k \log N_k)$, which is independent of the number of OFDM symbols N_p.

During the coarse sensing, since the number of subcarriers is much larger than the number of receive antennas and OFDM symbols, the complexity mainly comes from the operations along the fast time domain, i.e., the angle-DFT repeated on all subcarriers and the range estimation along fast time domain.

The complexity of solving the least-square problem in (24) is $\mathcal{O}(N_c N_t^2)$, and thus the detection of private subcarriers in N_s subcarriers has time complexity of $\mathcal{O}(N_s N_c N_t^2)$. The latency of detecting the private subcarriers is fixed, and is independent of the number of private subcarriers.

TABLE I
SYSTEM PARAMETERS

Parameter	Symbol	Value
Center frequency	f_c	28 GHz
Subcarrier spacing	Δf	120 kHz
Duration of OFDM symbol	T_p	8.92μs
Number of subcarriers	N_s	2048
Number of OFDM symbols	N_p	256
Number of radar receive antennas	N_r	32
Number of communication receive antennas	N_c	64
Receive antenna spacing distance	g_r	0.5λ
Transmit antenna spacing distance	g_t	0.5λ

VI. NUMERICAL RESULTS

In this section, we demonstrate the sensing and communication performance of the proposed DFRC-SS via simulations. The data symbols were modulated by 16QAM. The wideband system parameters were taken from the 5G NR high-frequency standard [53], and are shown in Table I.

The communication channels were simulated as follows. As in the radar case (see (4)), the signal transmitted between the n-th transmit antenna and the ℓ-th receive antenna undergoes an effect that can be modeled as propagation through a tap delay channel. The delay $\tau_{n\ell}$, is due to the direct path from the DFRC transmitter, i.e.,

$$\tau_{n\ell} = (R_c + n g_t \sin\theta + \ell d_r \sin\phi)/c, \tag{45}$$

where θ and ϕ are angles of departure and incidence, respectively.

The corresponding frequency response can be written as [6]

$$\mathbf{H}_i = \beta e^{-j2\pi i \Delta f R_c/c} \mathbf{a}_t(\theta, i)\mathbf{a}_r^T(\phi, i) + \sum_k c_k \mathbf{a}_t(\theta_k, i)\mathbf{a}_r^T(\phi_k, i), \tag{46}$$

where θ_k, ϕ_k are angles of departure and incidence related to the various scatterers, respectively, and c_k are the corresponding coefficients which were generated as complex random variables with mean 0.1 and variance 0.01. The summation term is the contribution of multiple non-resolvable paths, and guarantees the full rank of $\mathbf{H}_i$. In our simulations, we assumed that the summation contains N_t terms.

A. Precoder Design

In this section we obtain the precoder that minimizes the loss function of (44), and show the corresponding SNR gain with different number of transmit antennas. In this case we assumed $M = 8$ private subcarriers.

The desirable beam power profile was set to be 0 everywhere except over the angle range $[-52, -37]$ degrees, corresponding to the region of interest for the radar, and over the angle range $[29, 31]$ degrees, corresponding to the region where the communication receiver is located; over those angles the beam profile was set to 1. The weights γ_k were set to be 1×10^{-3} over all angles grids. If we set larger weights over certain area, we can better approximate the desired beampattern within that area, but we will have less control over other areas. For example, if we assign larger weights to the mainbeam, the sidelobe level will

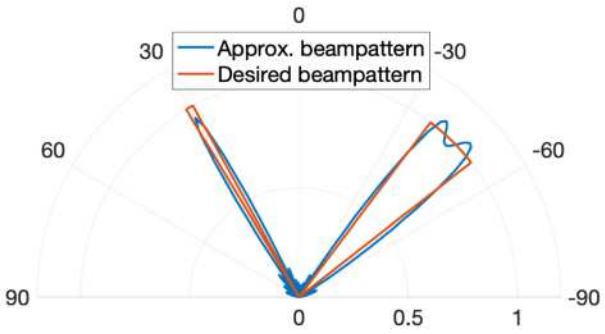

Fig. 3. Beampattern based on $N_t = 16$ transmit antennas.

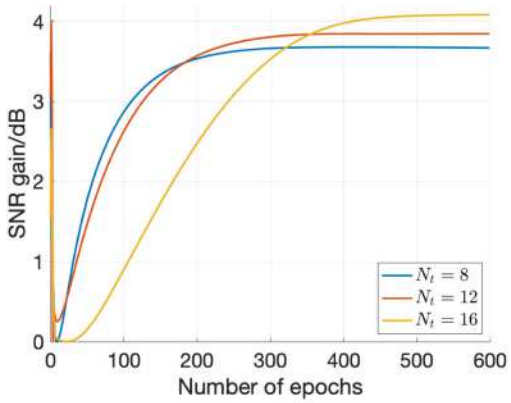

Fig. 4. SNR gains with 8, 12 and 16 transmit antennas.

increase. The weight in the total loss function of (44) was taken as $\alpha_b = 0.2$.

The optimum precoding matrix minimizes a weighted combination of the beampattern error, with respect to a desirable beampattern, and the inverse SNR at the communication receiver. Fig. 3, shows the designed beampattern for $N_t = 16$ antennas. Fig. 4 shows the variation of SNR during the iterations with respect to the minimal values for different numbers of transmit antennas. One can see that more transmit antennas result in higher SNR gain but also slower convergence. In the same figure, one can see that the SNR drops rapidly in the first 10 iterations, and then increases slowly and reaches convergence. Despite the small weight assigned to the beampattern error, in the beginning, the optimizer first aims to reduce the beampattern error, focusing less on improving the SNR. We observed the same behavior throughout our experiments, as long as the beampattern was randomly initialized. The corresponding learning curves for different numbers of transmit antennas are shown in Fig. 5. Based on Fig. 5, a larger number of transmit antennas leads to higher SNR gain and lower beampattern error upon convergence, but according to Fig. 4 the convergence is slower.

1) Peak-to-Average Power Ratio: An important issue in the proposed system, as in all OFDM systems, is the peak-to-average power ratio (PAPR) of the transmitted signal. The transmitted OFDM signal has a non-constant envelope and exhibits peaks whose power strongly exceeds the mean power. To avoid distortions of the transmitted signal, the transmit amplifier must operate in its linear regions. Therefore, power amplifiers with a

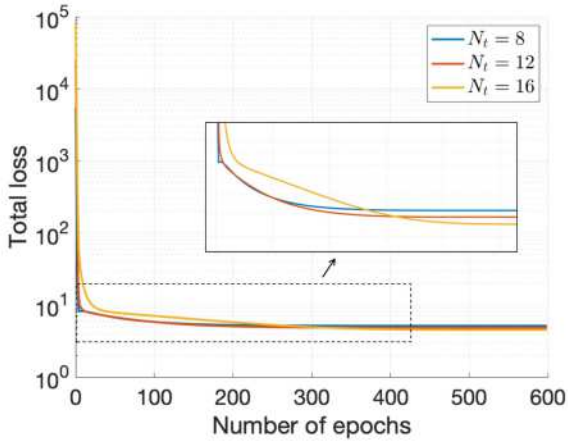

Fig. 5. The loss curves during optimization.

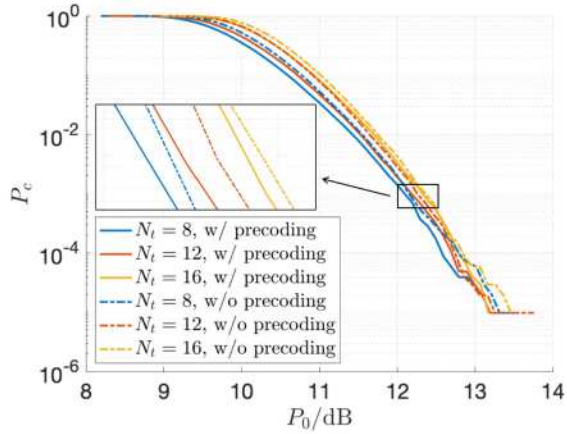

Fig. 6. PAPR of the proposed DFRC-SS system.

large dynamic range are required in OFDM systems which are expensive.

Here, PAPR is characterised by its complementary cumulative distribution function (CCDF) P_c, which is expressed as [65] $P_c = \Pr\{\text{PAPR} > P_0\}$. In other words, P_c counts for the probability that PAPR exceeds a particular value of P_0.

The transmit antennas transmit precoded OFDM signals. How the PAPR of OFDM signals behaves with the number of subcarriers, and how it can be mitigated is well-known [66]. Here, we investigate the effect of the precoding matrix, $\mathbf{P} \in \mathbb{C}^{N_t \times N_t}$ on the PAPR. The PAPR of the precoded OFDM signals using 16QAM is shown in Fig. 6 for different values of N_t. In each OFDM symbol, the maximum PAPR among the N_t antennas is recorded. For each value of N_t, the PAPR CCDF was computed based on 400 trials, 256 random OFDM symbols in each one. The PAPR of the same DFRC-SS OFDM system but without precoding is also shown in Fig. 6 using dot-dashed lines. Since we recorded the maximum PAPR among all transmit antennas, with more antennas the PAPR will also be higher. Based on the figure, one can see that the precoded signal has a slightly lower PAPR than the plain OFDM signals.

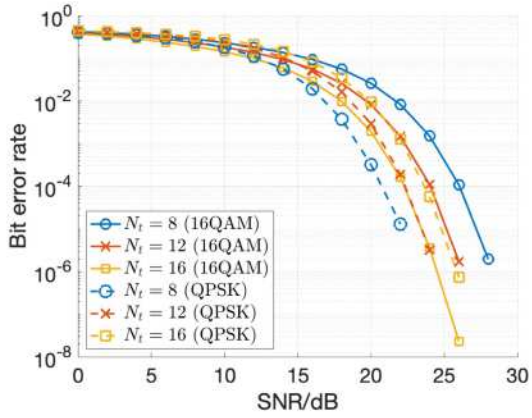

Fig. 7. Bit error rate on the shared subcarriers for different number of transmit antennas.

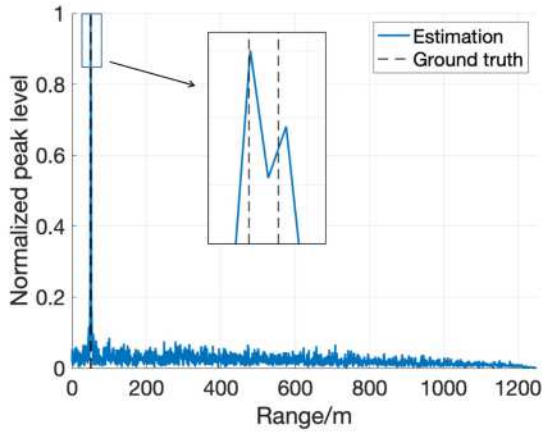

Fig. 8. Range cross-correlation result of two closely placed targets.

TABLE II
TARGETS PARAMETERS

Angles	Ranges	Velocities
$-43°$	$50m$	$13m/s$
$-43°$	$51m$	$20m/s$
$-46°$	$45m$	$-10m/s$
$-48°$	$100m$	$10m/s$

TABLE III
ESTIMATION RESULTS

Coarse estimation	Refined estimation	Velocity estimation
$(-43.43°, 50.05m)$	$(-43°, 50.05m)$	$11.73m/s$
$(-43.43°, 50.05m)$	$(-43°, 50.05m)$	$21.12m/s$
$(-48.59°, 100.10m)$	$(-46°, 100.10m)$	$-9.38m/s$
$(-48°, 45.17m)$	$(-48°, 45.17m)$	$9.39m/s$

B. Sensing and Communication Using All Subcarriers

Here we continue with the same system used in the previous subsection.

A communication receiver with $N_c = 64$ receive antennas was considered. The channels were simulated following (46), where the communication receiver is at distance $R_c = 50$ meters from the radar transmitter. For the direct path between the transmitter and communication receiver, the departure angle was $30°$ and the incident angle was $-45°$. The channel coefficients followed the same distribution as in the radar channel. The departure and incidence angles of scatters were random numbers, ranging from $-90°$ to $90°$ and the corresponding coefficients, c_k, were random complex numbers with mean equal to 0.1 and variance equal to 1×10^{-2}.

We assumed that the channels can be estimated at the communication receiver, which can be accomplished with pilots. We recovered the data symbols and mapped them back to binary bits via 16QAM demodulation. The bit error rate (BER) of the proposed DFRC-SS system on the shared subcarriers under different SNRs and with different number of transmit antennas is shown in Fig. 7. The BER performance with quadrature phase shift keying (QPSK) modulation is also shown in Fig. 7. The SNR was varied from 0 dB to 30 dB with a step size of 2 dB. One can see that on the shared subcarriers, 16QAM had a higher error than QPSK. For QPSK, BER grows with N_t, while for for 16QAM it decreases with N_t.

As for the corresponding sensing performance, we considered 4 point targets in the far field of the radar array, at angles, ranges, and velocities as shown in Table II. We should note that based on the aperture of the receive array of 32 antennas, these targets fall into 2 different angle bins; each bin has 2 targets at different ranges. The SNR was set to be 15 dB, and the channel coefficients, β_k, of (7) were assumed to be unknown. In this experiment, the transmitter had $N_t = 8$ antennas and the corresponding precoding matrix $\mathbf{P}$ was found by optimizing the criterion of (44).

1) Coarse Angle Estimation: Following the target parameter estimation described in Section II, we first obtained coarse target angle estimates based on the physical array of $N_r = 32$ antennas, using all (shared and private) subcarriers. As one can see, due to the low angle resolution of the receive array, only 2 different angle bins were found, i.e., angles $-43.43°$ and $-48.59°$, with each bin containing 2 targets. Subsequently, within each angle bin, target ranges were estimated via (13)–(17). The results are shown in Fig. 10 in red asterisks, while the ground truth is shown in black circles. Fig. 8 shows the cross-correlation result of range estimation (see (17)) in the angle bin $-43.43°$. One can clearly see two peaks at 50.05 m and 51.27 m, while the ground truth is 50 m and 51 m. As shown in Fig. 10, all 4 obtained ranges corresponding to the obtained angle bins are correct, but the angle estimates are not matched correctly with the targets especially the one at $-46°$ which is estimated to be $-48.59°$. The target radial velocities were estimated based on the corresponding range peaks (20) based on $N_p = 256$ OFDM symbols; the results are shown in Table III.

The standard deviation (STD) for cross-correlation based range and Doppler estimates is shown in Fig. 9, along with the CRB of the range related frequency $\omega_r(q, \mu)$ (see (15)) and velocity related Doppler frequency. Here we adopted the CRB of frequency estimation given in [67]. Range and Doppler estimation are based on finding peaks in the cross-correlation domain. By properly setting the detection threshold, the proposed method can be robust to noise levels, as shown in Fig. 9. One can see that the STD performance does not improve with SNR.

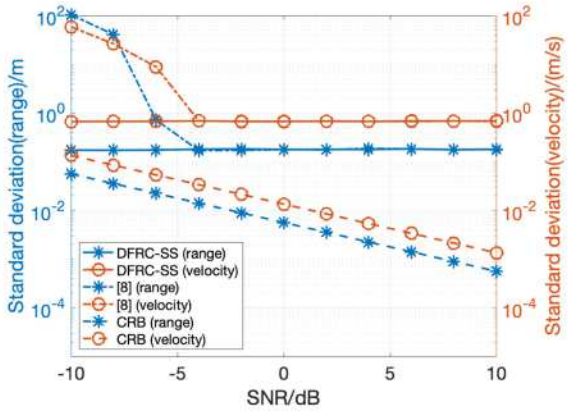

Fig. 9. Standard deviation of cross-correlation based range and Doppler estimation.

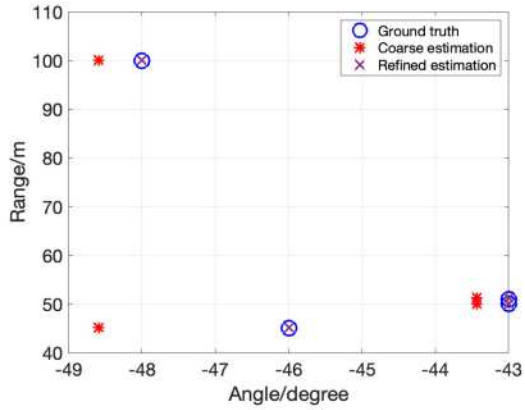

Fig. 10. Target estimation results before and after trading off communication for sensing via private subcarriers.

For the range, the performance will improve with the increase of bandwidth, since the resolution of the proposed range estimation method depends on the overall bandwidth (see Section II-B). Also, the velocity STD could only improve with using more OFDM symbols or a longer symbol duration (see Section II-C). However, during an extended observation time, the target may move out of the range bin. Increasing the symbol duration could improve the velocity resolution, but it would also reduce the maximum detectable velocity.

We also compared the sensing performance of the proposed method with that of [8], in which all subcarriers are private. In that case, target parameters are no longer coupled with transmitted data symbols, and the phase shifts due to range and velocity are orthogonal. Thus, after element-wise division with the transmitted symbol, range and velocity can be independently estimated via DFT and IDFT operations along the fast and slow time domains, respectively. The corresponding STD of range and velocity are shown in Fig. 9. As one can see, our proposed estimation method has the same performance as that of [8] when the SNR is high, while it is more robust to noise. Since in our method the range and Doppler estimation is carried out based on the angle-DFT peaks, the proposed method enjoys the beamforming gain from the receiver array which makes it more robust to noise. On the other hand, the method of [8] directly and individually estimates range and Doppler. When all subcarriers are used as shared, the proposed system can achieve a bit rate N_t times that in [8].

2) Angle Refinement Using a Virtual Array: Next we use the signals received on the the private subcarriers to refine the radar parameters obtained based on all (shared and private) subcarriers. For the same radar targets setup, we consider the case where $M = N_t = 8$ private subcarriers are used and the loss of communication rate is 0.39%.

We used the received signal on the private subcarriers, and also the target parameter estimates obtained above to formulate a virtual array. Following Section III-A, we first formulated an SSR problem using the 4 range estimates. In the formulated SSR problem, only the angle space near the two occupied angle bins was discretized. The SSR solution provided a sparse vector whose support indicated 3 angle bins at $-43°$, $-46°$ and $-48°$. The obtained angles were matched to the columns of the base matrix (see (34)), and thus to the ranges obtained so far. Based on that matching we found the angle-range pairs shown in Table III. The results are also shown in Fig. 10 marked by purple crosses. Re-estimating the ranges based on those angles did not change the results.

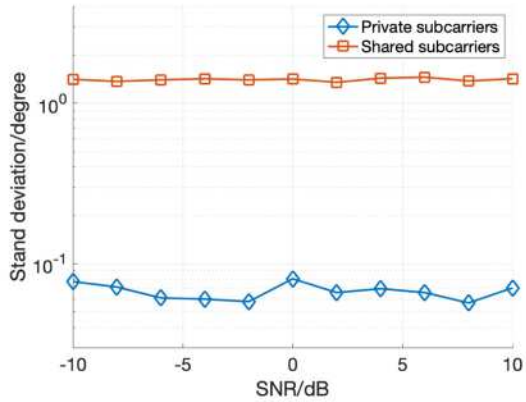

Fig. 11. Standard deviations of coarse angle estimates obtained based on all subcarriers, and refined ones obtained based on the private subcarriers.

In order to quantify the improvement of angle estimation due to the use of private subcarriers, Monte Carlo experiments were conducted with 4 private subcarriers under different SNR settings. 500 experiments were repeated for each SNR. In each experiment, 1 target was randomly generated and detected. The performances of cross-correlation based range and Doppler estimations were also investigated. As shown in Fig. 11, the STD of angle estimation, after trading off 14.4 Megabits/s for 4 private subcarriers, is much smaller than that of coarse angle estimation based on the physical receive array. Although the use of private subcarriers is at a cost of communication rate, the improvement in sensing performance is significant.

3) Trade-Off: In order to evaluate the trade-off between radar performance and communication rate in DFRC-SS, 500 Monte Carlo experiments were conducted with different numbers of

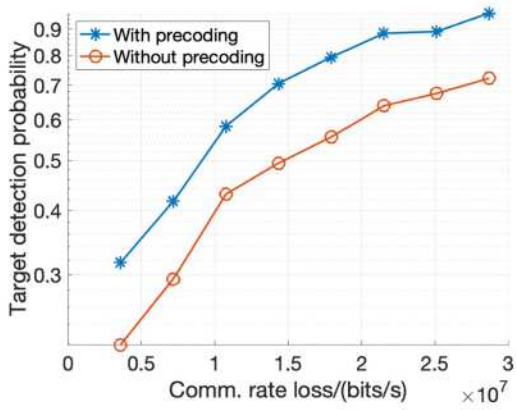

Fig. 12. Communication-sensing trade-off with and without precoding.

private subcarriers, or equivalently, different levels of communication rate loss. The number of private subcarriers varied from 1 to 8. In each experiment, 6 point targets were randomly placed between $-52°$ and $-37°$ (the area covered by the radar beam) and were detected following the approach proposed in Section III-A with different numbers of private subcarriers. The probability of successful detection, where all targets were detected and estimated correctly, is shown in Fig. 12. The same probability but for the case without precoding is also shown in Fig. 12. From the figure, one can see that the target estimation can recover most of the targets when the number of private subcarriers approaches the number of transmit antennas. Also, the designed precoder improves the detection probability.

Although the loss of communication rate is approximately 3.59 Megabits/s for each private subcarrier, the private subcarriers help improve the sensing performance. Under the current configuration, when $M = 8$, there would be about 7.57×10^{21} combinations of private subcarriers which requires 73 bits, i.e., 19 data symbols to encode the locations of private subcarriers. In addition, to encode the pairing between private subcarriers and transmit antennas, if there are $N_t = 8$ transmit antennas, 16 more bits, i.e., 4 more data symbols would be needed. However, if the private subcarriers were chosen to convey pilots, this information would have to be transmitted anyway to ensure that the receiver can know where the pilots are.

Under the configuration provided in the Table I, the maximum bit rate of the system is 14.694 Gigabits per second, when $N_t = 16$ antennas are used and all subcarriers are shared, while the loss of bit rate due to the use of private subcarriers is 7.175 Megabits per second per private subcarrier.

VII. Conclusion

We have proposed a novel DFRC system, that achieves high communication rate, and can flexibly trade-off bit rate for improved sensing performance. The proposed system is a monostatic MIMO radar that transmits wideband, precoded OFDM waveforms, and makes efficient use of the available bandwidth for communication and sensing by allowing antennas to simultaneously transmit on multiple subcarriers. The system subcarriers are divided into two groups, shared and private. When all subcarriers are used as shared the system fully utilizes the available bandwidth for communication and thus achieves high communication rate. Increasing the number of private subcarriers improves the sensing performance but reduces the communication rate. However, our simulation results showed that only a small number of subcarriers is needed to achieve the maximum sensing performance. We have proposed a novel and computationally simple method to estimate the target parameters, by first operating on all (shared and private) subcarriers to obtain coarse angle estimates, and then by fine-tuning those estimates based on the signal received on the private subcarriers. The proposed estimation approach, taking advantage of the high bandwidth available provides high-resolution angle, range and Doppler estimates. We have also proposed a precoder that is optimally designed to minimize a weighted combination of the beampattern error, with respect to a desirable beampattern, and the SNR at the communication receiver. The private subcarriers could be used to transmit pilot symbols for channel estimation.

Acknowledgment

The authors would like to thank the associate editor and anonymous reviewers for their insightful comments, and Prof. Joseph Tabrikian for useful discussions.

References

[1] W. Saad, M. Bennis, and M. Chen, "A vision of 6G wireless systems: Applications, trends, technologies, and open research problems," *IEEE Netw.*, vol. 34, no. 3, pp. 134–142, May/Jun. 2020.
[2] C. de Lima et al., "6G white paper on localization and sensing," University of Oulu, no. 12, 2020.
[3] A. Babaei, W. H. Tranter, and T. Bose, "A practical precoding approach for radar/communications spectrum sharing," in *Proc. IEEE 8th Int. Conf. Cogn. Radio Oriented Wireless Netw.*, 2013, pp. 13–18.
[4] H. Wang, J. Johnson, C. Baker, L. Ye, and C. Zhang, "On spectrum sharing between communications and air traffic control radar systems," in *Proc. IEEE Radar Conf.*, 2015, pp. 1545–1550.
[5] B. Li, A. P. Petropulu, and W. Trappe, "Optimum co-design for spectrum sharing between matrix completion based MIMO radars and a MIMO communication system," *IEEE Trans. Signal Process.*, vol. 64, no. 17, pp. 4562–4575, Sep. 2016.
[6] J. A. Zhang et al., "An overview of signal processing techniques for joint communication and radar sensing," *IEEE J. Sel. Topics Signal Process.*, vol. 15, no. 6, pp. 1295–1315, Nov. 2021.
[7] X. Chen, Z. Feng, Z. Wei, F. Gao, and X. Yuan, "Performance of joint sensing-communication cooperative sensing UAV network," *IEEE Trans. Veh. Technol.*, vol. 69, no. 12, pp. 15545–15556, Dec. 2020.
[8] C. Sturm and W. Wiesbeck, "Waveform design and signal processing aspects for fusion of wireless communications and radar sensing," *Proc. IEEE*, vol. 99, no. 7, pp. 1236–1259, Jul. 2011.
[9] Z. Feng, Z. Fang, Z. Wei, X. Chen, Z. Quan, and D. Ji, "Joint radar and communication: A survey," *China Commun.*, vol. 17, no. 1, pp. 1–27, Jan. 2020.
[10] P. Kumari, J. Choi, N. G. Prelcic, and R. W. Heath, "IEEE 802.11ad-based radar: An approach to joint vehicular communication-radar system," *IEEE Trans. Veh. Technol.*, vol. 67, no. 4, pp. 3012–3027, Apr. 2018.
[11] R. C. Daniels, E. R. Yeh, and R. W. Heath, "Forward collision vehicular radar with IEEE 802.11: Feasibility demonstration through measurements," *IEEE Trans. Veh. Technol.*, vol. 67, no. 2, pp. 1404–1416, Feb. 2018.
[12] E. Cianca, M. D. Sanctis, and S. D. Domenico, "Radios as sensors," *IEEE Internet Things J.*, vol. 4, no. 2, pp. 363–373, Apr. 2017.
[13] S. Sun, A. Petropulu, and H. V. Poor, "MIMO radar for ADAS and autonomous driving: Advantages and challenges," *IEEE Signal Process. Mag.*, vol. 37, no. 4, pp. 98–117, Jul. 2020.

[14] K. V. Mishra, M. R. B. Shankar, V. Koivunen, B. Ottersten, and S. A. Vorobyov, "Toward millimeter-wave joint radar communications: A signal processing perspective," *IEEE Signal Process. Mag.*, vol. 36, no. 5, pp. 100–114, Sep. 2019.

[15] H. Wymeersch, G. Seco-Granados, G. Destino, D. Dardari, and F. Tufvesson, "5G mmWave positioning for vehicular networks," *IEEE Wireless Commun.*, vol. 24, no. 6, pp. 80–86, Dec. 2017.

[16] Z. Xu, A. Petropulu, and S. Sun, "A joint design of MIMO-OFDM dual-function radar communication system using generalized spatial modulation," in *Proc. IEEE Radar Conf.*, 2020, pp. 1–6.

[17] F. Liu, C. Masouros, A. Petropulu, H. Griffiths, and L. Hanzo, "Joint radar and communication design: Applications, State-of-the-Art, and the road ahead," *IEEE Trans. Commun.*, vol. 66, no. 6, pp. 3834–3862, Jun. 2020.

[18] A. Hassanien, M. G. Amin, E. Aboutanios, and B. Himed, "Dual-function radar communication systems: A solution to the spectrum congestion problem," *IEEE Signal Process. Mag.*, vol. 36, no. 5, pp. 115–126, Sep. 2019.

[19] J. A. Zhang, M. L. Rahman, X. Huang, Y. J. Guo, S. Chen, and R. W. Heath, "Perceptive mobile network: Cellular networks with radio vision via joint communication and radar sensing," *IEEE Veh. Technol. Mag.*, vol. 16, no. 2, pp. 20–30, Jun. 2021.

[20] A. Hassanien, M. G. Amin, Y. D. Zhang, and F. Ahmad, "Signaling strategies for dual-function radar communications: An overview," *IEEE Aerosp. Electron. Syst. Mag.*, vol. 31, no. 10, pp. 36–45, Oct. 2016.

[21] F. Liu, L. Zhou, C. Masouros, A. Li, W. Luo, and A. Petropulu, "Toward dual-functional radar-communication systems: Optimal waveform design," *IEEE Trans. Signal Process.*, vol. 66, no. 16, pp. 4264–4279, Aug. 2018.

[22] D. Ma, N. Shlezinger, T. Huang, Y. Liu, and Y. C. Eldar, "Joint radar-communication strategies for autonomous vehicles: Combining two key automotive technologies," *IEEE Signal Process. Mag.*, vol. 37, no. 4, pp. 85–97, Jul. 2020.

[23] E. Uhlemann, "Time for autonomous vehicles to connect [Connected vehicles]," *IEEE Veh. Technol. Mag.*, vol. 13, no. 3, pp. 10–13, Sep. 2018.

[24] M. Di Renzo, H. Haas, A. Ghrayeb, S. Sugiura, and L. Hanzo, "Spatial modulation for generalized MIMO: Challenges, opportunities, and implementation," *Proc. IEEE*, vol. 102, no. 1, pp. 56–103, Jan. 2014.

[25] T. Huang, N. Shlezinger, X. Xu, Y. Liu, and Y. C. Eldar, "MAJoRCom: A dual-function radar communication system using index modulation," *IEEE Trans. Signal Process.*, vol. 68, pp. 3423–3438, 2020.

[26] K. Wu, J. A. Zhang, X. Huang, Y. J. Guo, and R. W. Heath, "Waveform design and accurate channel estimation for frequency-hopping MIMO radar-based communications," *IEEE Trans. Commun.*, vol. 69, no. 2, pp. 1244–1258, Feb. 2021.

[27] W. Baxter, E. Aboutanios, and A. Hassanien, "Dual-function MIMO radar-communications via frequency-hopping code selection," in *Proc. IEEE 52nd Asilomar Conf. Signals, Syst., Comput.*, 2018, pp. 1126–1130.

[28] J. Euziére, R. Guinvarc'h, M. Lesturgie, B. Uguen, and R. Gillard, "Dual function radar communication time-modulated array," in *Proc. IEEE Int. Radar Conf.*, 2014, pp. 1–4.

[29] X. Wang, A. Hassanien, and M. G. Amin, "Dual-function MIMO radar communications system design via sparse array optimization," *IEEE Trans. Aerosp. Electron. Syst.*, vol. 55, no. 3, pp. 1213–1226, Jun. 2019.

[30] D. Ma et al., "Spatial modulation for joint radar-communications systems: Design, analysis, and hardware prototype," *IEEE Trans. Veh. Technol.*, vol. 70, no. 3, pp. 2283–2298, Mar. 2021.

[31] A. Ali, N. Gonzalez-Prelcic, R. W. Heath, and A. Ghosh, "Leveraging sensing at the infrastructure for mmWave communication," *IEEE Commun. Mag.*, vol. 58, no. 7, pp. 84–89, Jul. 2020.

[32] Y. Liu, G. Liao, Z. Yang, and J. Xu, "Multiobjective optimal waveform design for OFDM integrated radar and communication systems," *Signal Process.*, vol. 141, pp. 331–342, 2017. [Online]. Available: https://www.sciencedirect.com/science/article/pii/S0165168417302360

[33] F. Liu, C. Masouros, A. Li, H. Sun, and L. Hanzo, "MU-MIMO communications with MIMO radar: From co-existence to joint transmission," *IEEE Trans. Wireless Commun.*, vol. 17, no. 4, pp. 2755–2770, Apr. 2018.

[34] Z. Ni, J. A. Zhang, K. Yang, X. Huang, and T. A. Tsiftsis, "Multi-Metric Waveform Optimization for Multiple-Input Single-Output Joint Communication and Radar Sensing," *IEEE Trans. Commun.*, vol. 70, no. 2, pp. 1276–1289, 2022, doi: 10.1109/TCOMM.2021.3132368.

[35] Y. Rong, A. R. Chiriyath, and D. W. Bliss, "MIMO radar and communications spectrum sharing: A multiple-access perspective," in *Proc. IEEE 10th Sensor Array Multichannel Signal Process. Workshop*, 2018, pp. 272–276.

[36] Y. Liu, G. Liao, and Z. Yang, "Range and angle estimation for MIMO-OFDM integrated radar and communication systems," in *Proc. IEEE CIE Int. Conf. Radar*, 2016, pp. 1–4.

[37] G. N. Saddik, R. S. Singh, and E. R. Brown, "Ultra-wideband multifunctional communications/radar system," *IEEE Trans. Microw. Theory Techn.*, vol. 55, no. 7, pp. 1431–1437, Jul. 2007.

[38] D. Gaglione, C. Clemente, C. V. Ilioudis, A. R. Persico, I. K. Proudler, and J. J. Soraghan, "Fractional Fourier based waveform for a joint radar-communication system," in *Proc. IEEE Radar Conf.*, 2016, pp. 1–6.

[39] A. Hassanien, M. G. Amin, Y. D. Zhang, and F. Ahmad, "Dual-function radar-communications using phase-rotational invariance," in *Proc. IEEE 23rd Eur. Signal Process. Conf.*, 2015, pp. 1346–1350.

[40] Y. Liu, G. Liao, J. Xu, Z. Yang, and Y. Zhang, "Adaptive OFDM integrated radar and communications waveform design based on information theory," *IEEE Commun. Lett.*, vol. 21, no. 10, pp. 2174–2177, Oct. 2017.

[41] S. H. Dokhanchi, M. R. B. Shankar, T. Stifter, and B. Ottersten, "OFDM-based automotive joint radar-communication system," in *Proc. IEEE Radar Conf.*, 2018, pp. 0902–0907.

[42] G. Duggal, S. Vishwakarma, K. V. Mishra, and S. S. Ram, "Doppler-resilient 802.11ad-based ultrashort range automotive joint radar-communications system," *IEEE Trans. Aerosp. Electron. Syst.*, vol. 56, no. 5, pp. 4035–4048, Oct. 2020.

[43] C. Xu, B. Clerckx, S. Chen, Y. Mao, and J. Zhang, "Rate-splitting multiple access for multi-antenna joint radar and communications," *IEEE J. Sel. Topics Signal Process.*, vol. 15, no. 6, pp. 1332–1347, Nov. 2021.

[44] R. Nee, V. Jones, G. Awater, A. V. Zelst, J. Gardner, and G. Steele, "The 802.11n MIMO-OFDM standard for wireless LAN and beyond," *Wireless Pers. Commun.*, vol. 37, pp. 445–453, 2006.

[45] Y. Li, M. Zhang, W. Zhu, M. Cheng, C. Zhou, and Y. Wu, "Performance evaluation for medium voltage MIMO-OFDM power line communication system," *China Commun.*, vol. 17, no. 1, pp. 151–162, Jan. 2020.

[46] M. Ergen, *Mobile Broadband - Including WiMAX and LTE*, 1st ed. Berlin, Germany: Springer, 2009.

[47] Y. Liu, G. Liao, and Z. Yang, "Robust OFDM integrated radar and communications waveform design based on information theory," *Signal Process.*, vol. 162, pp. 317–329, 2019. [Online]. Available: https://www.sciencedirect.com/science/article/pii/S0165168419301598

[48] Y. Liu, G. Liao, Y. Chen, J. Xu, and Y. Yin, "Super-resolution range and velocity estimations with OFDM integrated radar and communications waveform," *IEEE Trans. Veh. Technol.*, vol. 69, no. 10, pp. 11659–11672, Oct. 2020.

[49] M. F. Keskin, V. Koivunen, and H. Wymeersch, "Limited feedforward waveform design for OFDM dual-functional radar-communications," *IEEE Trans. Signal Process.*, vol. 69, pp. 2955–2970, 2021.

[50] J. Tabrikian, "Performance bounds and techniques for target localization using MIMO radars," in *MIMO Radar Signal Processing*, J. Li and P. Stoica, Eds. New York, NY, USA: Wiley, 2008, ch. 4, pp. 153–189.

[51] N. I. Miridakis and D. D. Vergados, "A survey on the successive interference cancellation performance for single-antenna and multiple-antenna OFDM systems," *IEEE Commun. Surveys Tuts.*, vol. 15, no. 1, pp. 312–335, Jan.–Mar. 2013.

[52] L. Hanzo, M. Münster, B. Choi, and T. Keller, *OFDM and MC-CDMA for Broadband Multi-User Communications, WLANs and Broadcasting*. New York, NY, USA: Wiley, 2003. [Online]. Available: https://eprints.soton.ac.uk/258228/

[53] Y. Wang, C. Qi, P. Li, Z. Lu, and P. Lu, "Channel estimation for wideband mmWave MIMO OFDM system exploiting block sparsity," *IEEE Commun. Lett.*, vol. 26, no. 4, pp. 897–901, Apr. 2022.

[54] D. Bao, G. Qin, J. Cai, and G. Liu, "A precoding OFDM MIMO radar coexisting with a communication system," *IEEE Trans. Aerosp. Electron. Syst.*, vol. 55, no. 4, pp. 1864–1877, Aug. 2019.

[55] C. B. Barneto et al., "Full-duplex OFDM radar with LTE and 5G NR waveforms: Challenges, solutions, and measurements," *IEEE Trans. Microw. Theory Techn.*, vol. 67, no. 10, pp. 4042–4054, Oct. 2019.

[56] E. Aboutanios and B. Mulgrew, "Iterative frequency estimation by interpolation on Fourier coefficients," *IEEE Trans. Signal Process.*, vol. 53, no. 4, pp. 1237–1242, Apr. 2005.

[57] J. Li and P. Stoica, "MIMO radar with colocated antennas," *IEEE Signal Process. Mag.*, vol. 24, no. 5, pp. 106–114, Sep. 2007.

[58] D. S. Kalogerias and A. P. Petropulu, "Matrix completion in colocated MIMO radar: Recoverability, bounds amp; theoretical guarantees," *IEEE Trans. Signal Process.*, vol. 62, no. 2, pp. 309–321, Jan. 2014.

[59] R. G. Baraniuk, "Compressive sensing [Lecture notes]," *IEEE Signal Process. Mag.*, vol. 24, no. 4, pp. 118–121, Jul. 2007.

[60] J. Xu, G. Liao, S. Zhu, L. Huang, and H. So, "Joint range and angle estimation using MIMO radar with frequency diverse array," *IEEE Trans. Signal Process.*, vol. 63, no. 13, pp. 3396–3410, Jul. 2015.
[61] M. D. Larsen, A. L. Swindlehurst, and T. Svantesson, "Performance bounds for MIMO-OFDM channel estimation," *IEEE Trans. Signal Process.*, vol. 57, no. 5, pp. 1901–1916, May 2009.
[62] Z. Xu and A. P. Petropulu, "DFRC with improved communication-sensing trade-off via private subcarrier permutations and pairing with antennas," in *Proc. IEEE Wireless Commun. Netw. Conf.*, 2022, pp. 245–250.
[63] D. P. Kingma and J. Ba, "Adam: A method for stochastic optimization," in *Proc. 3rd Int. Conf. Learn. Representations*, San Diego, CA, USA, May 7–9, 2015. [Online]. Available: http://arxiv.org/abs/1412.6980
[64] B. Ghazi, H. Hassanieh, P. Indyk, D. Katabi, E. Price, and L. Shi, "Sample-optimal average-case sparse Fourier transform in two dimensions," in *Proc. IEEE 51st Annu. Allerton Conf. Commun., Control, Comput.*, 2013, pp. 1258–1265.
[65] W. Shieh and I. Djordjevic, "Chapter 2 - OFDM principles," in *OFDM for Optical Communications*, W. Shieh and I. Djordjevic, Eds. Oxford, U.K.: Academic Press, 2010, pp. 31–52. [Online]. Available: https://www.sciencedirect.com/science/article/pii/B9780123748799000022
[66] Y. A. Jawhar et al., "A review of partial transmit sequence for PAPR reduction in the OFDM systems," *IEEE Access*, vol. 7, pp. 18021–18041, 2019.
[67] D. Rife and R. Boorstyn, "Single tone parameter estimation from discrete-time observations," *IEEE Trans. Inf. Theory*, vol. 20, no. 5, pp. 591–598, Sep. 1974.

Zhaoyi Xu (Graduate Student Member, IEEE) received the B.E degree in electrical engineering from the University of Electronic Science and Technology of China, Chengdu, China, in 2018. He is currently working toward the Ph.D. degree in electrical engineering with the ECE Department, Rutgers University, New Brunswick, NJ, USA, with professor Athina Petropulu. His research interests include radar signal processing, sparse array design, dual-function radar communication system design, and remote vital signal monitoring.

Athina P. Petropulu (Fellow, IEEE) is currently a Distinguished Professor with the Electrical and Computer Engineering (ECE) Department, Rutgers, and was the Chair of the Department during 2010–2016. Prior to joining Rutgers, she was a Professor of ECE, Drexel University, Philadelphia, PA, USA, during 1992–2010. She held a Visiting Scholar appointments with SUPELEC, Universite' Paris Sud, Orsay, France, Princeton University, Princeton, NJ, USA, and University of Southern California, Los Angeles, CA, USA. Her research interests include statistical signal processing, wireless communications, signal processing in networking, physical layer security, and radar signal processing. Her research has been funded by various government industry sponsors, including the National Science Foundation, Office of Naval research, U.S. Army, National Institute of Health, Whitaker Foundation, Lockheed Martin and Raytheon. Dr. Petropulu is Fellow of the American Association for the Advancement of Science, and was recipient of the 1995 Presidential Faculty Fellow Award given by NSF and White House. She is 2022-2023 President of the IEEE Signal Processing Society (SPS) and 2020 President-Elect of IEEE SPS. She was the Editor-in-Chief of the IEEE TRANSACTIONS ON SIGNAL PROCESSING during 2009–2011 and IEEE Signal Processing Society Vice President-Conferences during 2006–2008. She was the General Chair of 2020 and 2021 IEEE SPS PROGRESS Workshops, General Co-Chair of the 2018 IEEE International Workshop on Signal Processing Advances in Wireless Communications (SPAWC), Kalamata Greece, and General Chair of the 2005 International Conference on Acoustics Speech and Signal Processing (ICASSP-05), Philadelphia, PA, USA. She was a Distinguished Lecturer of IEEE Signal Processing Society and IEEE Aerospace & Electronics Systems Society. She was the recipient of the 2012 IEEE Signal Processing Society Meritorious Service Award, and corecipient of the 2005 IEEE Signal Processing Magazine Best Paper Award, 2020 IEEE Signal Processing Society Young Author Best Paper Award (B. Li), 2021 IEEE Signal Processing Society Young Author Best Paper Award (F. Liu), 2021 Barry Carlton Best Paper Award by IEEE Aerospace and Electronic Systems Society, and 2022 IEEE Sensor Array and Multichannel Signal Processing Workshop Best Student paper Award (Y. Li).